International Journal of Mechanical and Materials Engineering (IJMME), Vol. 4 (2009), No. 1, 62 -69.

NUMERICAL STUDY OF THE HEAT TRANSFER AUGMENTATION IN PIPES WITH INTERNAL DISCONTINOUS LONGETUDINAL FINS

Khalid M. Saqr[1] and Md N. Musa[2]

[1] High-Speed Reacting Flow Laboratory, Faculty of Mechanical Engineering
[2] Department of Thermofluids, Faculty of Mechanical Engineering,
Universiti Teknologi Malaysia, 81310 Skudai, Johor Bahru - MALAYSIA
Email: mmdmskhalid2@siswa.utm.my

ABSTRACT

Internally finned (i.e. ribbed) pipes are ideal to be used in flow-based waste heat recovery applications, where the internal heat transfer coefficient has a radical effect on the overall application efficiency. Such pipes provide significantly higher heat transfer coefficient than plain pipes. Compared to helically finned pipes, pipes with internal longitudinal fins have lower pressure drop. The principal objective of this paper is to investigate the effect of repetitive fin discontinuity on the convective heat transfer coefficient for pipes with internal longitudinal fins. A CFD model was used to study the heat transfer augmentation resulting from disturbing the thermal boundary layer by repetitive discontinuities in the fin lateral profile. The CFD model was validated against published empirical correlations for internally finned pipes with compressible viscous flow. Stanton number, Nusselt number and the convective heat transfer coefficient are computed for three different geometries at constant heat transfer coefficient on the outer wall. The effects of both continuous and discontinuous fins on heat transfer are elucidated. A new correlation to predict the temperature drop per unit length as a function of discontinuity offset distance is presented.

Keywords: *Internal Longitudinal Fins, CFD, Enhanced Heat Transfer, Turbulent flow*

NOMENCLATURE

D_h	Hydraulic diameter (m)
D_O	Outer diameter (m)
D_{md}	Meltdown diameter (m)
Nu_{DB}	Dittus-Boelter Nusselt number
Re	Reynolds Number
A_{md}	Meltdown area (m^2)
T_f	Fin thickness (m)
S	Offset distance (m)
L_P	Pipe length (m)
P	Pressure (Pa)
f	Friction factor
D_i	Inner diameter (m)
D_r	Root diameter (m)
H_f	Fin height (m)
β	Helix angle
Pr	Prandtl number
N	Number of fins
k	Thermal conductivity of fluid
P_h	Helix pitch (m)
w	Discontinuity distance (m)
ρ	Density (kg/m^3)
m	Mass flow rate (kg/s)

1 INTRODUCTION

1.1 Literature Review

Heat transfer and flow dynamics in pipes with internal longitudinal fins have enjoyed intensive concern of both mathematical and experimental research in the last four decades (Kern & Kraus, 1972). These concerns resulted from the realization of the heat transfer enhancement achieved by such ribs and their important applications in heat exchangers, hence, reducing the heat exchanger size. Although the experimental data for different geometries and flow regimes have been reported in previous literature, only one set of predictive correlations for the Nusselt number and friction factor have been formulated (Webb et al, 1994; Bergles, 1998; Bejan & Kraus, 2003) . Although the utilization of longitudinal ribs in circular ducts has proved to dramatically enhance the convective heat transfer, it is quite imperative to emphasize that it increases the pressure drop effectively as well.

Prior studies have focused on helical and transverse ridging, as firstly studied in 1971 (Webb et al, 1971). Nine years later, the study was extended to include the effect of helix angle (i.e. pitch) on the heat transfer coefficient and friction factor (Gee & Webb, 1980). In fact, helical ribs are

quite different, in terms of geometry, from discontinues longitudinal fins, as illustrated in the schematic cross section in Figure 1. Longitudinal fins prevail over the helical fins by providing larger heat transfer surface area. Nonetheless, continues longitudinal fins do not provide the turbulence generating effect that exists in helical fins. For this reason, discontinuous fins are expected to create turbulence while maintaining a large surface area.

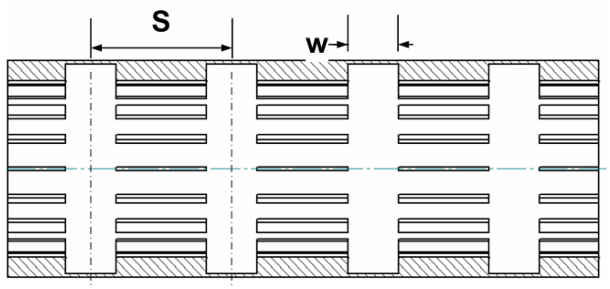

(a)

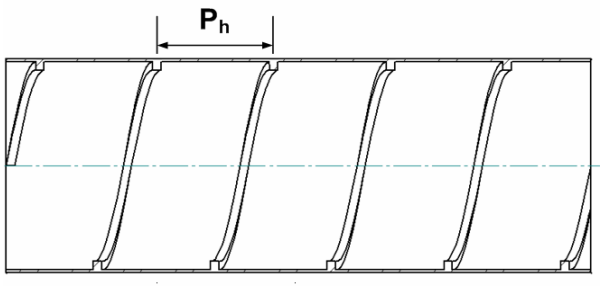

(b)

Figure 1 (a) Internal longitudinal fins with axial discontinuities (b) Internal helical fins

1.2 Objectives of the Present Study

For laminar viscous flow, the enhancement in heat transfer is not as effective as in turbulent flow if the pressure drop in both cases is taken into consideration. The empirical correlations presented by Carnavos in 1979 for predicting Nusselt number and convective heat transfer coefficient for ducts with longitudinal continuous fins take into account the effect of fin geometry on the heat transfer area as well as on the friction factor (Carnavos, 1979). There are two objectives for this study, first to establish and validate a CFD model of turbulent compressible flow inside pipes having longitudinal continuous fins, through a comparison with the abovementioned empirical correlations. Second objective is to implement the validated model to investigate the enhancement in convective heat transfer when the axial profile of the fins is subjected to repetitive discontinuities at different offset distances. The empirical equations and the CFD model are explained in the second section followed by the results and discussion in the third section. Concluding remarks are presented finally.

2 MATHEMATICAL ANALYSES

2.1 Empirical Equations

The selected equations were derived through experimental investigation on 21 different tube geometries. The experimental tests included both axial and helical internal fins with helix angles up to 30°. The Carnavos experimental fluid database includes water, air, and an ethylene glycol/water mixture, the developed Nusselt number correlation is a function of the Dittus-Boelter Nusselt number and fin geometry (Carnavos, 1979):

$$Nu_C = Nu_{DB}\left(D_i D_{md}^{-1} - 2H_f D_{md}^{-1}\right)^{-0.2}\left(D_i D_h D_{md}^{-2}\right)^{0.5} Sec^3\beta \quad (1)$$

The term D_{md} was described in (Wolverine, 2001) as *"the diameter which would exist if the fins were melted down and added to the internal perimeter of the tube"*. On the other hand, the same term was described in (Bejan & Kraus, 2003) as "*the fin envelope internal area"*. The 'meltdown diameter' can be mathematically expressed as:

$$D_{md} = \sqrt{\frac{4}{\pi}A_{md}} = \sqrt{\frac{4}{\pi}NH_f T_f} \quad (2)$$

The dimensions in equations (1) and (2) are illustrated in Figure 2. The angle β is considered as 0º in case of longitudinal straight fins. The Dittus-Boelter correlation (Dittus & Boelter, 1930) for calculating the Nusselt number is:

$$Nu_{DB} = 0.023\,\mathrm{Re}_d^{0.8}\,\mathrm{Pr}^n \quad (3)$$

The overall internal heat transfer coefficient is expressed as a function of the Nusselt number calculated from Carnavos correlation as follows:

$$\alpha_C = \frac{Nu_C k}{D_h} \quad (4)$$

The hydraulic diameter is expressed as:

$$D_h = \frac{4 \times Flow\ cross\ \ section\ area}{Perimeter} = \frac{\pi D_r^2 - 4NH_f T_f}{\pi D_r + N\left(2H_f + T_f\right)} \quad (5)$$

On the other hand, the friction factor is expressed as a function of the Blasius friction factor and fin geometry:

$$f = f_{Blasius}\left(\frac{D_{md}}{D_r}\right)Sec^{0.75}\beta \quad (6)$$

$$f_{Blasius} = \frac{0.046}{\mathrm{Re}^{0.2}} \quad (7)$$

The friction factor should be used in the flow equation to calculate the pressure drop along the pipe, a simple form of the flow equations is:

$$\Delta P = \frac{2 f \dot{m}^2 L_P}{\rho D_h} \quad (8)$$

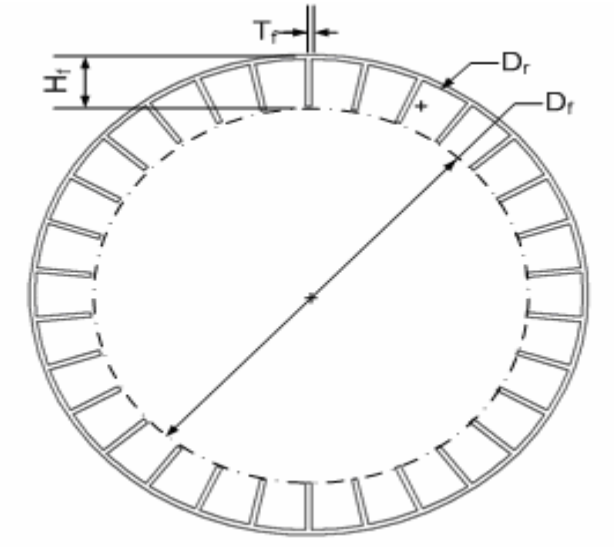

(a)

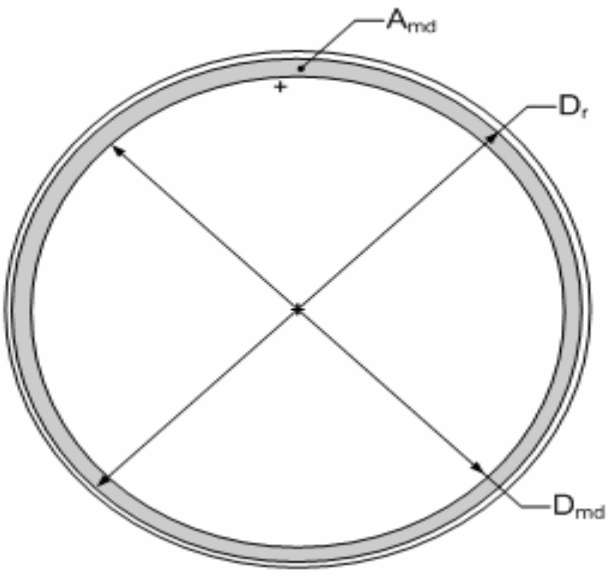

(b)

Figure 2 (a) A cross section in the hot-side heat exchanger showing the internal longitudinal fins (b) The virtual meltdown area and diameter

2.2 Governing Equations of the CFD model

The air flow inside longitudinally finned pipe can be described by the favre-averaged Navier-Stokes equations. The averaged form of continuity, momentum, and energy equations for a steady state, axisymmetric and compressible flow can be expressed as follows respectively:

$$\frac{\partial \overline{\rho}\,\overline{u}_i}{\partial x_i} = 0 \tag{9}$$

$$\frac{\partial \rho \bar{u}_j \bar{u}_i}{\partial x_j} = -\frac{\partial \bar{p}}{\partial x_i} + \frac{\partial}{\partial x_i}\left[\bar{t}_{j_i} - \overline{\rho u_i' u_j'}\right] \tag{10}$$

$$\frac{\partial}{\partial x_j}\left[\overline{\rho u}_j\left(\bar{h} + \frac{\bar{u}_i^{\,2}}{2}\right) + \bar{u}_j\,\frac{\overline{u_i' u_j'}}{2}\right] = \frac{\partial}{\partial x_j}\left[-ql_j - \overline{\rho u_j h} + \overline{t_{j_i} u'}_i - \overline{\rho u_j \frac{u_i^{\,2}}{2}}\right] + \frac{\partial}{\partial x_j}\left[\bar{u}_i\left(\bar{t}_{j_i} - \overline{\rho u_i' u_j'}\right)\right] \tag{11}$$

where $\bar{u}$ is the mean velocity component in x_i direction, p is the mean pressure, $\bar{t}_{j_i}$ is the molecular shear stress, and h is the specific enthalpy. The overbar denotes favre (mass) averaging, and the prime denotes fluctuating component. In this study k-ε turbulence model is used for closure of the governing equations because of its robustness and low computational expense (Launder & Spalding, 1972).

2.3 Standard k-ε Turbulence Model

Generally, k-ε models solve two additional transport equations - one for the turbulent kinetic energy and the other is for the turbulent dissipation rate. These models uses Boussinesq hypothesis which proposes that the transport of momentum by turbulence is a diffusive process and thus the Reynolds stresses ($-\overline{u_i' u_j'}$) can be modelled using turbulent (eddy) viscosity which is analogous to molecular viscosity.

$$-\overline{u_i' u_j'} = 2\upsilon_t\left(\frac{\partial \bar{u}_i}{\partial x_j} + \frac{\partial \bar{u}_j}{\partial x_i}\right) - \frac{2}{3}k\,\delta_{ij} \tag{12}$$

In the standard k-ε model (Launder & Spalding, 1972), the turbulence kinetic energy and turbulence dissipation rate are obtained from the following modeled transport equations:

$$u_j\frac{\partial k}{\partial x_j} = \tau_{tij}\frac{\partial u_i}{\partial x_j} - \varepsilon + \frac{\partial}{\partial x_j}\left[\nu + \upsilon_t/\sigma_k\,\frac{\partial k}{\partial x_j}\right] \tag{13}$$

$$u_j\frac{\partial \varepsilon}{\partial x_j} = C_{\varepsilon 1}\frac{\varepsilon}{k}\tau_{tij}\frac{\partial u_i}{\partial x_j} - C_{\varepsilon 2}\frac{\varepsilon^2}{k} + \frac{\partial}{\partial x_j}\left[\nu + \upsilon_t/\sigma_\varepsilon\,\frac{\partial \varepsilon}{\partial x_j}\right] \tag{14}$$

$$\upsilon_t = C_\mu k^2/\varepsilon \tag{15}$$

where υ_t is the turbulent viscosity and k-ε model empirical coefficients have the following values (Launder & Spalding, 1972).

$C_{1\varepsilon} = 1.44, C_{2\varepsilon} = 1.92, C_{\mu} = 0.09$

$\sigma_k = 1.0 \; and \; \sigma_{\varepsilon} = 1.3$

3 SIMULATION FEATURES

3.1 Pipe Geometry

The first model for the CFD analysis represents a pipe with continuous longitudinal fins, for the purpose of model validation. While there are five different pipe geometries having discontinuous fins, each of them has a different offset distance for the fin discontinuity. The dimension symbols are as illustrated in Figures 1 and 2. The dimension values for the six models are featured in Table 1. Model 1 is used for the validation purpose, while models 2 to 6 are used to investigate the effect of fins discontinuity on the convective heat transfer.

Table 1: Dimensions of the pipe models used in the CFD analysis

Dimension	Models					
(m)	1	2	3	4	5	6
L_P	0.50	0.25	0.25	0.25	0.25	0.25
S	0	0.02	0.03	0.04	0.05	0.06
w	0	0.015	0.015	0.015	0.015	0.015
T_f	6×10^{-4}	6×10^{-4}	6×10^{-4}	6×10^{-4}	6×10^{-4}	6×10^{-4}
N	20	20	20	20	20	20
H_f	0.004	0.004	0.004	0.004	0.004	0.004
D_r	0.0508	0.0508	0.0508	0.0508	0.0508	0.0508

3.2 Solver Details

The CFD solver in COSMOSFloworks® commercial package offers fully automatic mesh generation of complex geometries with local, user-defined, adaptive refinement for both solid and fluid cells. Furthermore, it offers automatic treatment of boundary layers and an automatic handling of $\times10^{-9}$laminar, turbulent and transitional flow regimes within one model (Weinhold & Mlynski, 2004; Pavlov. 2007) The software discretises the time-dependent Navier-Stokes equations and solves them on a variable density computational mesh with rectangular shape. The equations are supplemented by fluid state equations defining the nature of the fluid, and by empirical dependencies of fluid viscosity and/or thermal conductivity on temperature. The software employs the standard k-ε model to calculate the turbulent kinetic energy and its dissipation rate, which are necessary to take into account the Reynolds stresses term appears in the equations as a result of applying the Average Favre-average Navier-Stokes solution procedure (Pavlov, 2007; NIKA Gmbh, 2007), which is a density weighted variant of the Reynolds-average Navier Stokes (RANS) approach.

3.3 Meshing and boundary conditions

For the model validation analysis, the constant fluid and solid cell sizes were set to 2.4×10^{2} mm^3. As for the discontinuous fin models, an adaptive meshing approach was employed throughout the flow region in order to optimize the boundary layer effect and to obtain higher resolution results in this region. The maximum and minimum cell sizes were set to 37.8 mm^3 and 4.72×10^{-1} mm^3, respectively. In order to reduce the calculations time, the axisymmetric flow assumption was used to shrivel the computational domain to a 90^o longitudinal section of the pipe, as in Figure 3. In this computational domain, the total number of cells was limited to 145006 cells.

The boundary conditions for all cases used inlet mass flow rate at one end of the pipe, and ambient pressure and the other end. The outer convective heat transfer coefficient of the pipe was set to 6 W/m^2.K with an ambient temperature of 298 K. The inlet air temperature was fixed at 353 K for all analysis cases.

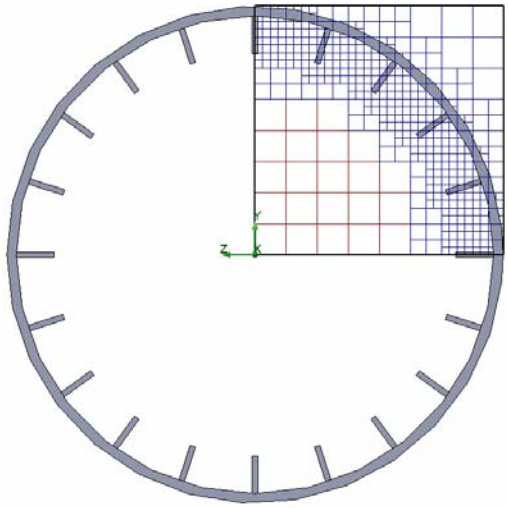

Figure 3. A 90^o computational domain contains the adapted mesh for the fin discontinuity analysis

4 RESULTS AND DISCUSSION

4.1 CFD model validation

In order to validate the CFD model, pressure drop was calculated using the empirical equations (6-8) and compared to the pressure drop computed from the CFD model. The CFD model slightly overpredicted both the average flow velocity and pressure drop along the pipe. The deficiencies of the k-ε turbulence model in modeling high-strain rate flows can be one major reason for such overpredictions.

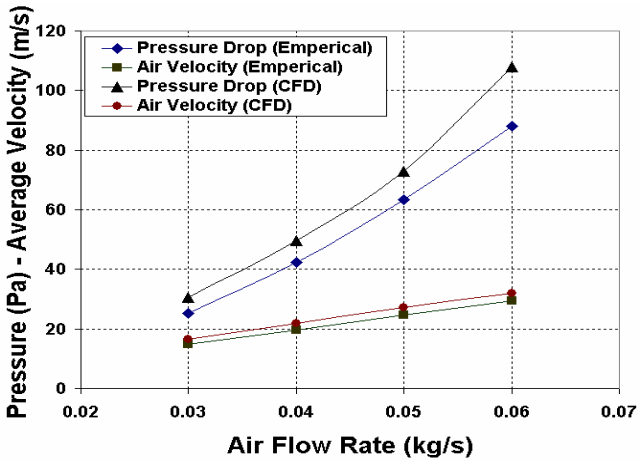

Figure 4. Comparison between empirical and CFD calculated pressure drop and average axial velocity

Table 2. Deviation between the pressure drop and air velocity calculated from empirical equations and CFD model

Flow rate (kg/s)	Deviation	
	ΔP	v
0.03	20.74%	11.17%
0.04	17.36%	11.33%
0.05	15.19%	10.16%
0.06	22.78%	8.2%

The high strain rate, in the case in hand, is attributed to the sharp, repetitive radial changes in the flow geometry, which impose large scale eddies to the turbulent flow field. And since the k-ε turbulence model is based on the Boussinesq hypothesis, which assumes that all turbulent eddies are isotropic (Wilcox, 1994), the model tends to overpredict such phenomena that are dominated by large scale eddies. However, the trend of pressure drop computed via CFD model for four different values of air flow rate, agrees with the same trend calculated using empirical equations. In addition, the average axial air velocity computed from the CFD model, shows similar agreement with the air velocity calculated from the empirical equations. The result of the validation comparison in presented in Figure 4.

From Table 2, it is evident that the CFD computed velocity shows more agreement with the empirical correlations. However, the maximum deviation of the CFD computed pressure drop from the empirical calculated one is not more than 23%.

4.2 Effect of internal continuous fins on heat transfer

Equations (1-5) were solved in order to determine the effect of internal longitudinal continuous fins on heat transfer, as in Figure 5. In Figure 5-a, the Stanton number is plotted against the air mass flow rate for a plain pipe and a finned pipe having fin length, thickness and number of 4 mm, 0.6mm and 20 respectively. The difference between the two curves indicates the positive effect on the convective heat transfer. In Figure 5-b, Stanton number is plotted against number of fins for a plain pipe and a finned one having fin length and thickness of 4 mm and 0.6 mm respectively, at a constant air mass flow rate of 0.04 kg/s.

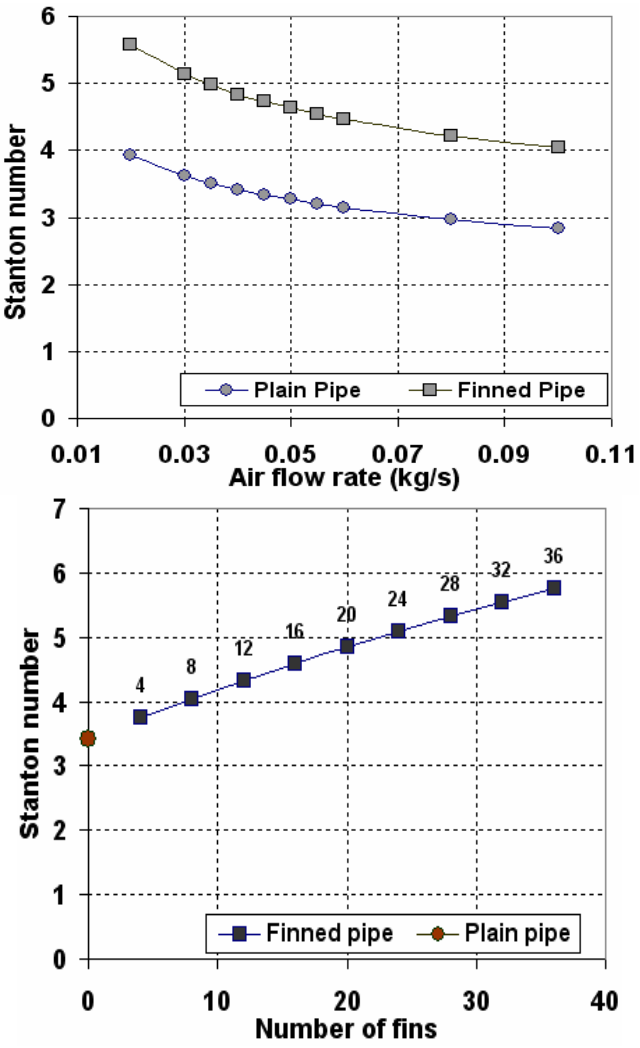

Figure 5. Stanton number vs. air mass flow rate for plain and internally finned pipes

The Stanton number exhibits significant increase at higher number of fins due to the increase in heat transfer area and flow velocity induced by the fins. In Figure 6, the effect of continuous fins on increasing the convection heat transfer is explained. It is can be seen that 40% increase in the convective heat transfer coefficient can be achieved using these fins. However, in low air mass flow rate, the enhancement in heat transfer is significantly less than 40%, because of the reduced air velocity.

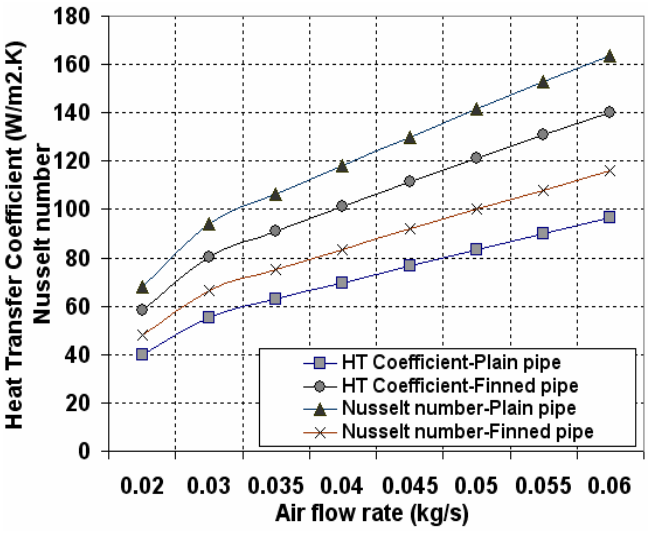

Figure 6. Effect of continuous fins on the heat transfer compared to plain pipe

The Nusselt number shows a very similar trend to the convective heat transfer coefficient because of the small pipe diameter, which permits only small changes in the transport properties of air, which maintain almost constant Prandtl number across the pipe diameter. In the same time, the air flow rate increases, along with a constant diameter. This boosts the average Reynolds number causing the abovementioned similarity between Nusselt number and convective heat transfer coefficient trends. On the other hand, when the convective heat transfer coefficient and Nusselt number are plotted against an increasing number of fins, as in Figure 7, their trends are observed to be different. The increasing number of fins obliges the meltdown diameter to decrease, consequently, the Nusselt number decreases as well. Alternatively, the hydraulic diameter will decrease significantly, which will increase the convective heat transfer coefficient. The intersection between the two curves denotes the number of fins at which the negative effect caused by the decreased Nusselt number, and the positive effect caused by the decreased hydraulic diameter equalize.

4.3 Effect of fin discontinuity of heat transfer augmentation

The air temperature pattern across the finned pipe is plotted in Figure 6 for different discontinuity offset distances. It is observed that the smaller the offset distance, the higher the temperature drop. The change in pipe geometry, which is represented in the fin discontinuity, when it is introduced at a larger repetition rate it increases the flow turbulence near the pipe walls. This induced turbulence enforces the thermally conductive boundary layer to be collided on the fins causing the convective heat transfer coefficient to increase substantially. On the other hand, a smaller repetition rate (i.e. larger offset distance) would allow the thermal conductive boundary layer to develop near the pipe walls. This thermally conductive fluid layer demonstrates insulating behavior, as heat is transferred through it by means of conduction, which is insignificant when it comes to fluids, air in this sense.

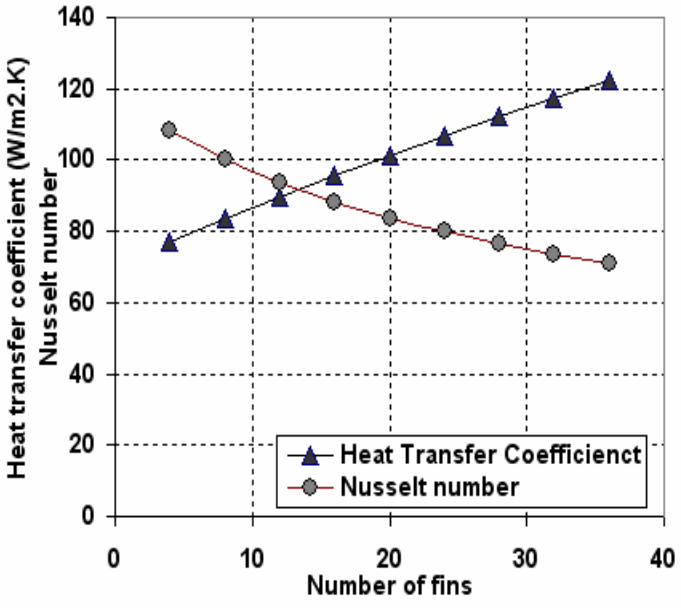

Figure 7. Nusselt number and convective heat transfer coefficient vs. number of fins

The average air temperature drop per pipe unit length is plotted against fin discontinuity offset distance in Figure 7. It is obvious that the augmentation in heat transfer is fairly significant compared to the change in offset distance. A pipe with the same number of continuous fins demonstrates an air temperature drop per pipe unit length of 7.4 K/m, at the same boundary conditions.

This data was used to derive a new correlation to predict the temperature drop per unit length as a function of the discontinuity offset distance, for pipes having discontinues longitudinal fins. The proposed correlation is:

$$\frac{dT}{L} = 26.62\ e^{-8.8876\ S} \qquad (16)$$

This correlation is valid for a ratio of the discontinuity distance to discontinuity offset distance $\left(\frac{w}{S}\right)$ of 0.136 to 1.33, and for a (S) value of 0.01 o 0.13 m.

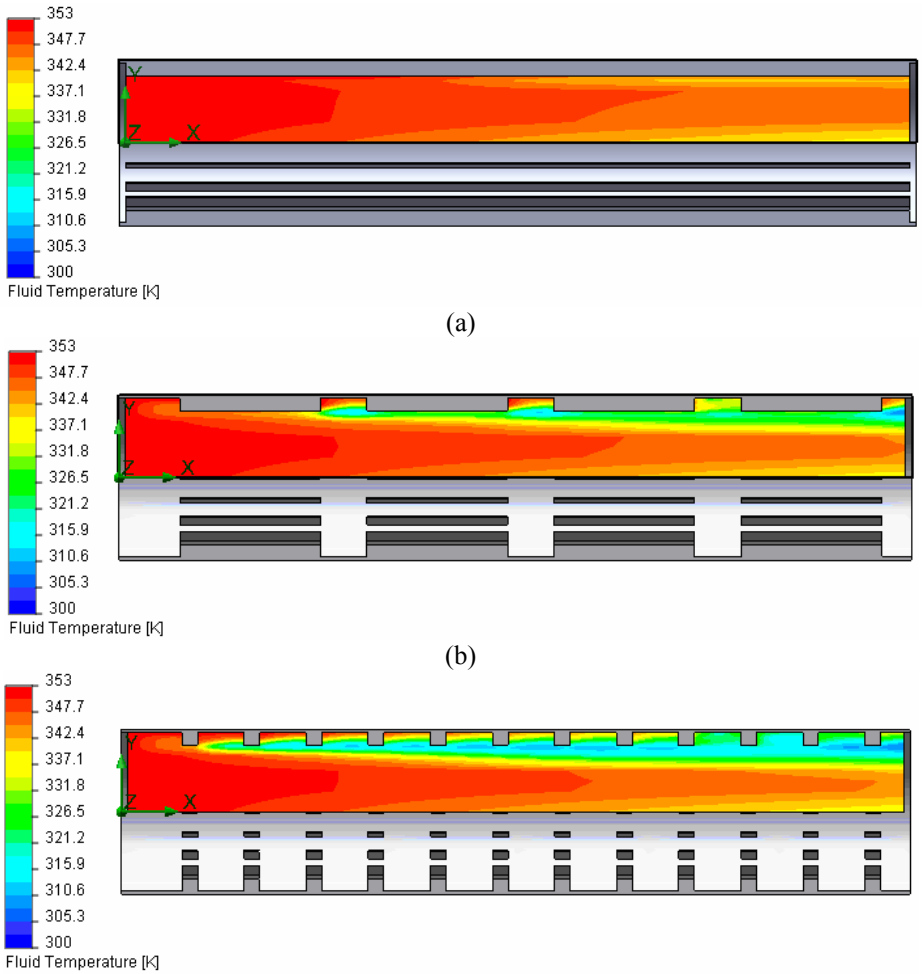

Figure 8. Fluid temperature profiles for internally finned pipe with discontinuity offset distance of (a) 0.0 m, (b) 0.06 m and (c) 0.02 m

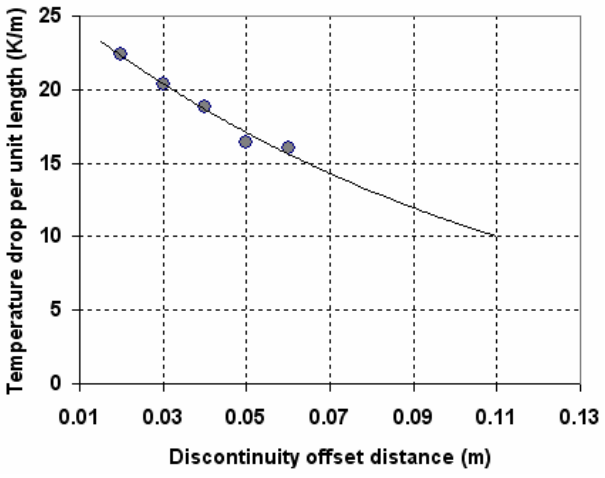

Figure 9. Average air temperature drop per unit length vs. discontinuity offset distance

5 CONCLUSIONS

A numerical investigation of the effect of continuous and discontinuous internal longitudinal fins on heat transfer augmentation for steady state, axisymmetric turbulent compressible flow has been conducted. The numerical model and solution were validated against established empirical correlations. Repetitive discontinuity along the fin profile showed to have radical effect on the internal convective heat transfer coefficient. It was found that the smaller the discontinuity offset distance, the higher the convective heat transfer coefficient. The main contribution of this study is the derivation of a new correlation to express the heat transfer augmentation in terms of temperature drop per unit length as a function of the fin discontinuity offset distance. Future work should verify the accuracy of this correlation, as well as its geometric limitations.

ACKNOLWLEDGMENT

Partial support for this work was provided by the Ministry of Science, Technology and Innovation (MOSTI) under Science Fund grant number 79060.

REFERNCES

Bejan A., and Kraus A. D. 2003 Heat Transfer Handbook, John Wiley and Sons Inc., Ch. 14 pp 1052-1064

Bergles, A. E. 1998 Techniques to Enhance Heat Transfer, in Handbook of Heat Transfer, 3rd ed., Rohsenow W. M., Hartnett, J. P., and Cho, Y. I., McGraw-Hill, New York, Ch. 11.

Carnavos, T. C. 1979 Heat Transfer Performance of Internally Finned Tubes in Turbulent Flow, in Advances in Heat Transfer, ASME, New York, pp. 61-67.

Dittus, F. W., and Boelter, L. M. K. 1930 Pub Eng., Univ. California (Berkeley) Vol. 2 p 443

Gee,D.L., and Webb,R.L. 1980 Forced convection heat transfer in helically rib-roughened tubes, Int. J. Heat and Mass Transfer, Vol.23, pp. 1127-1136,

Kern, D. Q., and Kraus, A. D. 1972 Extended Surface Heat Transfer, McGraw-Hill, New York.

Launder, B.N. and Spalding, D. B. , 1972 Lectures in Mathematical Models of Turbulence. Academic Press, London, England

NIKA GmbH, 2007 EFD.Lab® 5: Fundamentals, Available online at: http://www.nika.biz/PDFs/EFD.Lab_Fundamentals.pdf

Pavlov, V.V., 2007 Embedded CFD Aids Hydrodynamics Research, DE Online, September 4th. Available at:http://www.deskeng.com/articles/aaafbr.htm

Webb, R. L., Menze, K., Rudy, T., Ayub, Z., and Fujii, M. 1994 Technology Review, J. Enhanced Heat Transfer, Vol. 1(2), pp:127-130.

Webb,L., Eckert, E.R.G. and Goldstein, R.J., 1971 Heat transfer and friction in tubes with repeated-rib roughness, Int. J. Heat and Mass Transfer, Vol.14, pp. 601-617,

Weinhold, I., and Mlynski, G., 2004 Numerical simulation of airflow in the human nose, Eur Arch Otorhinolaryngol, 261: 452-455

Wilcox, D. C., 1994 Turbulence Modeling for CFD, DCW Industries, Inc. pp: 213-230

Wolverine Tube Inc. 2001 Engineering Data Book III, Ch. 5 Available at: http://www.wlv.com/products/databook/db3/DataBookIII.pdf